La mer 33, 135–147, 1995
Société franco-japonaise d'océanographie, Tokyo

A numerical study on the formation of circulations in the Yellow Sea during summer*

Satoru TAKAHASHI** and Tetsuo YANAGI**

Abstract: In the Yellow Sea during summer, YANAGI snd TAKAHASHI (1993) suggested that an anti-clokwise circulation was developed in the upper layer and a clockwise one in the lower layer. Generation mechanisms of these circulations are investigated using numerical model with two kinds of simplified model basin. Consequently, it is revealed that these circulations are mainly induced by the topographic heat accumulation effect. On the other hand, vertical temperature distribution is affected by the horizontal difference of vertical mixing induced by tidal current.

1. Introduction

The Yellow Sea is a shelf sea that is surrounded by the west coast of the Korean Peninsula and the east coast of China and is connected to the East China Sea through the southern open boundary. It is well known that the stratification is developed by the sea surface heating and the Yellow Sea Bottom Cold Water is formed at the deepest part of the Yellow Sea in summer (FUKASE, 1975; TAWARA and YAMAGATA, 1991; etc.).

Recently, YANAGI snd TAKAHASHI (1993) revealed the seasonal variation in circulation patterns in the Yellow Sea using diagnostic numerical model. In their summer results, an anti-clockwise circulation was devloped at the upper layer and a clokwise one at the lower layer in the central part of the Yellow Sea. They showed that these circulations were accompanied with the Yellow Sea Bottom Cold Water (YSBCW). CHOI and LIE (1992) showed the result of drifter buoys tracking during July to October, 1986. The tracks of surface buoys denoted an anti-clockwise circulation at the surface layer in the central part of the Yellow Sea. Furthermore, SU and WENG (1994) investigated the surface circulations in the Yellow Sea and the East China Sea using water mass analysis and suggested an anti-clockwise circulation at the central part of the Yellow Sea in summer. From these results the existence of an anti-clockwise (a clockwise) circulation at the upper (lower) layer in the central part of the Yellow Sea is suggested. However, the generation mechanisms of these circulations are still unknown. In the present study, we aim to reveal the generation mechanisms of an anti clockwise (at the upper layer) and a clockeise (at the lower layer) circulations in the Yellow Sea during summer.

Seasonal variation of temperature and salinity distributions along the vertical cross section in the central part of the Yellow Sea was investigated by TAWARA and YAMAGATA (1991).

The observation stations and the vertical distributions of temperature in August and April. are shown in Fig. 1 (TAWARA and YAMAGATA, 1991). In August, stratification is developed and the highest water temperature is found at the surface layer of the central part and YSBCW was fonud at the bottom layer in the deepest part.

CHOI (1984) showed the horizontal distribution of M_2 tidal current amplitude in the Yellow Sea and the East China Sea using numerical model. In the Yellow Sea, the strength of the tidal current at the deep central part is weaker than that at the surrounding shallow part, i. e., it is expected that the vertical mixing effect induced by tidal current at the deep central part is weaker than that at the surrounding shallow

*Received December 7, 1994
**Department of Civil and Ocean Engineering, Ehime University, Matsuyama, 790 Japan

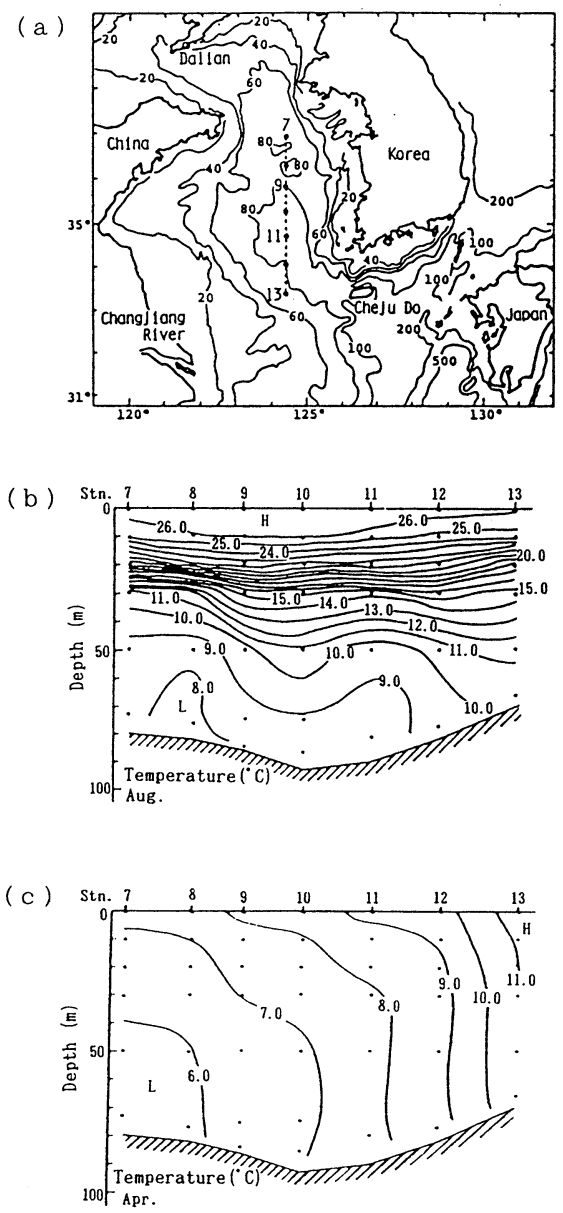

Fig. 1. Map of the observation stations (a) and vertical distributions of temperature in August (b) and in April (c) obtained by averaging data during 1977 to 1986, after TAWARA and YAMAGATA (1991).

part. This effect may have some influence on the water temperature distribution in the Yellow Sea.

From these results, we can consider that the effects of the bottom topography and the vertical mixing induced by the tidal current may contribute to the formation of the circulations and YSBCW in the Yellow Sea during summer. So, we carried out the numerical model experiments in which these effects are included.

2. Numerical model

2.1. Model basin and basic equation

Table 1 shows the heat fluxes through the sea surface (ISHII and KONDO, 1987) and those between the Yellow Sea and the East China Sea (ISHII and KONDO, 1993) during the heating season. Except March and August, vertical heat fluxes through the sea surface are larger about 3 times than the horizontal ones. So, as a first approximation, horizontal heat flux between the Yellow Sea and the East China Sea is ignored in this model, and in order to reveal the effect of the tidal mixing and the effect of the bottom topography to the generation of an anti clockwise and a clockwise circulations in the Yellow Sea during summer, two kinds of model basins which have a round shape are applied here. The bottom topography of the Yellw Sea (a) and the model regions (No. 1: (b), No. 2: (c)) are shown in Fig. 2. The No. 1 model basin has a constant depth (80 m) and No. 2 has a slope running along the coastal line in the model basin which represents the shelf slope in the Yellow Sea. This slope has a simple exponen-

Table 1. Heat fluxes through the sea surface and between the Yellow Sea and the East China Sea during heating period. After ISHII and KONDO (1987 and 1993).

	heat flux (I) (W)	heat flux (II) (W)
Mar.	1.2×10^{13}	-0.2×10^{13}
Apr.	5.7×10^{13}	1.5×10^{13}
May.	6.6×10^{13}	1.4×10^{13}
Jun.	7.3×10^{13}	1.1×10^{13}
Jul.	7.0×10^{13}	2.3×10^{13}
Aug.	5.2×10^{13}	3.6×10^{13}

heat flux (I): vertical heat flux through the sea surface
heat flux (II): horizontal heat flux between the Yellow Sea and the East China sea

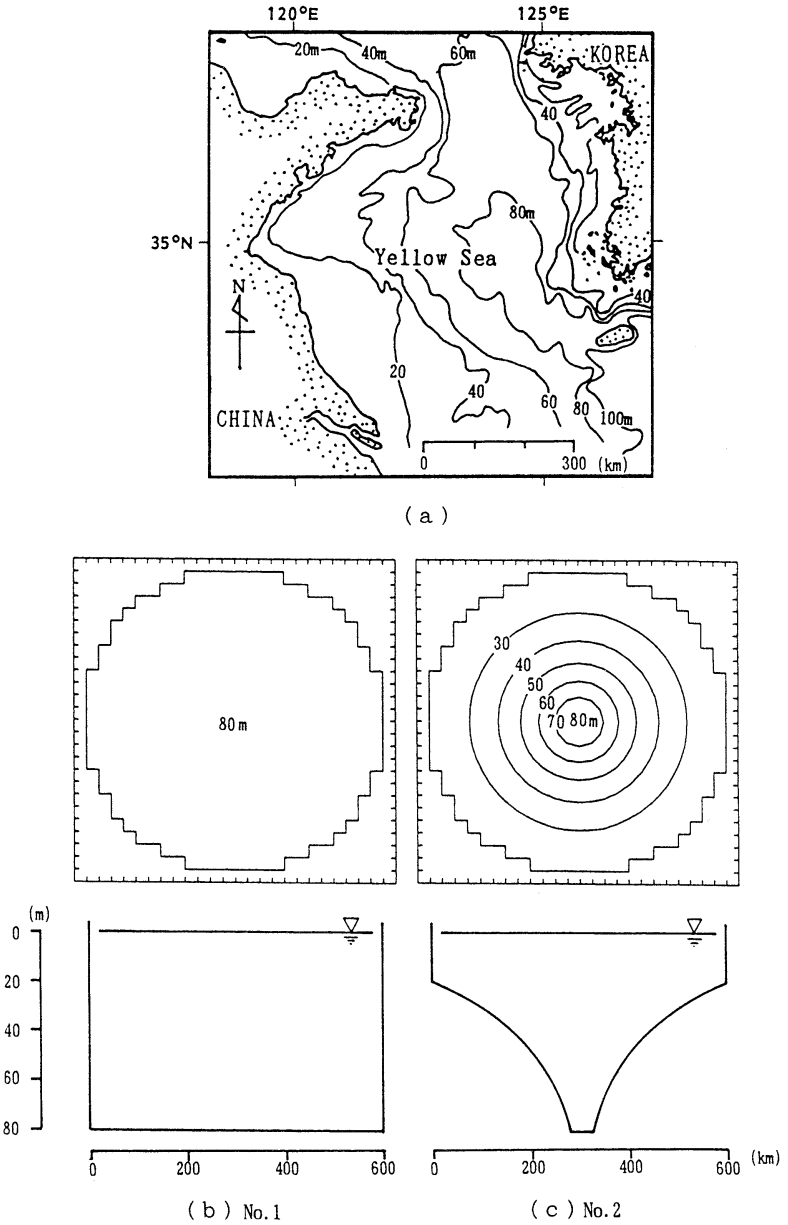

Fig. 2. Bottom topography of the Yellow Sea (a) and two model basins (b) (c).

tial form of $h = h_0 \exp(ax')$, where $h_0 = 20$ m, $a = 5.04 \times 10^{-6} (m^{-1})$ and x', is offshore distance from the coast in meter. The maximum depth of the No. 2 model basin is 80m. The horizontal grid size is 25km × 25km and the water column is vertically divided into four levels (level 1: 0–10m, level 2: 10–20m, level 3: 20–40m, level 4: 40 m–bottom).

Under the hydrostatic pressure, the Boussinesq and f-plain approximations, numerical model consists of the equations of motion, continuity and advection-diffusion of temperature. Using conventional notation, these equations on the Cartesian coordinate are as follows:

$$\frac{\partial u}{\partial t}+\left(u\frac{\partial u}{\partial x}+v\frac{\partial u}{\partial y}+w\frac{\partial u}{\partial z}\right)-fv = -\frac{1}{\rho_0}\frac{\partial P}{\partial x}+\frac{\partial}{\partial x}\left(A_h\frac{\partial u}{\partial x}\right)+\frac{\partial}{\partial y}\left(A_h\frac{\partial u}{\partial y}\right)+\frac{\partial}{\partial z}\left(A_v\frac{\partial u}{\partial z}\right) \quad (1)$$

$$\frac{\partial v}{\partial t}+\left(u\frac{\partial v}{\partial x}+v\frac{\partial v}{\partial y}+w\frac{\partial v}{\partial z}\right)+fu = -\frac{1}{\rho_0}\frac{\partial P}{\partial x}+\frac{\partial}{\partial x}\left(A_h\frac{\partial v}{\partial x}\right)+\frac{\partial}{\partial y}\left(A_h\frac{\partial v}{\partial y}\right)+\frac{\partial}{\partial z}\left(A_v\frac{\partial v}{\partial z}\right) \quad (2)$$

$$\frac{\partial P}{\partial z}=\rho g \quad (3)$$

$$\frac{\partial u}{\partial x}+\frac{\partial v}{\partial y}+\frac{\partial w}{\partial z}=0 \quad (4)$$

$$\frac{\partial T}{\partial t}+\left(u\frac{\partial T}{\partial x}+v\frac{\partial T}{\partial y}+w\frac{\partial T}{\partial z}\right) = K_h\left(\frac{\partial^2 T}{\partial x^2}+\frac{\partial^2 T}{\partial y^2}\right)+K_v\frac{\partial^2 T}{\partial z^2} \quad (5)$$

where u, v, and w are the velocity components of x, y and z directions, respectively, f (8.34×10^{-5} sec^{-1}) the Coriolis parameter at 35° N, t the time, P the pressure, ρ the water density, ρ_0 the reference density, g (980 cm/sec^2) the gravitational accelration, A_h and K_h the horizontal eddy viscosity and diffusivity, respectively, A_v and K_v the vertical eddy viscosity and diffusivity, respectively, and T the water temperature. The density is calculated from T and salinity with use of the usual nonlinear state equation (WADACHI, 1987). However, only the effect of heat on density is considered, here. So, from TAWARA snd YAMAGATA (1991), averaged salinity in heating season (33.0 psu) is applied.

The boundary condition for momentum is slip condition at all lateral walls. The bottom stress is given as follows,

$$A_v\frac{\partial u}{\partial z}=C_b u(u^2+v^2)^{1/2} \quad (6)$$

The sea surface is assumed to be a free-surface, and the sea surface heat flux is given as follows,

$$K_v\frac{\partial T}{\partial z}=\frac{Q_s}{C\rho} \quad (7)$$

Here, C_b (0.0026) is the bottom drag coefficient, Q_s the heat flux through the sea surface and C (0.932cal/℃/g) the specific heat of water. Using observation value of ISHII and KONDO (1987), Q_s is assumed as,

$$Q_s=350\sin(2\pi t/T_y). \quad (\text{cal/cm}^2\text{/day}) \quad (8)$$

Here, T_y is one year.

2.2. Procedure of the experiments

The circulations in the Yellow Sea during summer is expected to be induced by the sea surface heating during spring and summer because the wind in these seasons is very weak (YANAGI and TAKAHASHI, 1993). So, only Q_s is applied as a external force. We expect that the bottom topography of the Yellow Sea may affect the circulations. Thus, in order to investigate the effect of the bottom topogeaphy, two kinds of model basins (No. 1 and No. 2, see Fig. 2) are applied. Furthermore, we expect that the horizontal difference of vertical mixing due to the tidal current may affect the circulations. In order to investigate such effects, three kinds of vertical eddy diffusivities are applied. Here, in order to restrain the occurrence of the internal waves at the interface between upper and lower levels of the model basin, the verticl eddy viscosity which is some lager than the vertical eddy diffusivity is applied. Three kinds of vertical eddy diffusivities, corresponding vertical eddy viscosity and horizontal eddy diffusivity and viscosity are shown in the following.

1. The vertical eddy diffusivity is constant.
   The vertical eddy viscosity and diffusivity are given as

$$A_v=30 \text{ (cm}^2\text{/sec)}, \quad (9)$$
$$K_v=5 \text{ (cm}^2\text{/sec)}, \quad (10)$$

and horizontal eddy viscosity and diffusivity are also constant as

$$A_h=K_h=10^6 \text{ (cm}^2\text{/sec)}, \quad (11)$$

2. The vertical eddy diffusivity varies with exponential form.

From the tidal current amplitude chart of CHOI (1984), the vertical eddy viscosity and diffusivity are given as

$$A_v=10\exp(3.66\times10^{-8}x^*), \{\text{maximum : 20}\} \text{ (cm}^2\text{/sec)} \quad (12)$$
$$K_v=\exp(7.68\times10^{-8}x^*), \{\text{maximum : 10}\} \text{ (cm}^2\text{/sec)} \quad (13)$$

and horizontal eddy viscosity and diffusivity are given as

$$A_h = K_h = 10^5 \exp(7.68\times10^{-8}x^*), \quad \{\text{maximum} : 10^6\}\ (\text{cm}^2/\text{sec}) \qquad (14)$$

where x^* is the distance from the center point of the model basin in cm.

3. The vertical eddy diffusivity depends on the Richardson number (JAMES, 1977; TAKEOKA *et al*, 1991).

The vertical eddy viscosity is given as

$$A_v = K_v + 10,\ (\text{cm}^2/\text{sec}) \qquad (15)$$

and according to TAKEOKA *et al* (1991), the vertical eddy diffusivity are written as

$$K_v = \frac{K_0}{(1+\sigma Ri)^p} + K_b, \qquad (16)$$

where, K_0+K_b ($K_0=50.0$, $K_b=0.1$ cm^2/sec) is the diffusivity in well-mixed state, σ (25.0) and p (0.7) the constants which were determined by TAKEOKA *et al.* (1991) and Ri the Richardson number. K_b is the background diffusivity which is added to prevent K_v becoming too small for large Ri. The Richardson number is given by

$$Ri = g\alpha \frac{\partial T/\partial z}{V} \qquad (17)$$

Here, α (0.0002℃$^{-1}$) is the thermal expansion coeffcient and V the square of vertical shear of the horizontal velocity. Under the approximation of the logarithmic law for the vertical distributions of the tidal current and wind-induced current, V is written as

$$V = \frac{1}{2}\{\frac{u^*}{k(H-|z|)}\}^2 + (\frac{W^*}{kz})^2 + (\frac{\partial u}{\partial z})^2. \qquad (18)$$

The first term on the right-hand side is the contribution of the shear of the tidal current, the second term that of the wind-induced current and the third term that of the density-driven current. u^* and W* the friction velocities of the tidal current and the wind-induced current, respectively, and K (0.41) the Karmans constant. The friction velocities are given as

$$u^* = C_b^{1/2} u_a, \qquad (19)$$

$$W^* = (\rho_a/\rho)^{1/2} C_a^{1/2} W, \qquad (20)$$

where ρ_a (0.0012 kg/m^3) is the air density, C_a (0.0013) the drag coefficient at the sea surface, W (2.0 m/sec) the wind speed, and u_a is the tidal current amplitude, that is given from CHOI (1984) as

$$u_a = 120 - 20\exp\{0.477\times10-8\ (L/2-x^*)\}\ (\text{cm/sec}). \qquad (21)$$

Here L (600km) is the diameter of model basin. In this case, horizontal eddy viscosity and

Table 2. Cases of the experiments.

Case	Depth	*Kh, Ah*	*Kz, Az*
1	No. 1	exp	exp
2	No. 2	const	const
3	No. 2	exp	exp
4	No. 2	exp	*Ri*

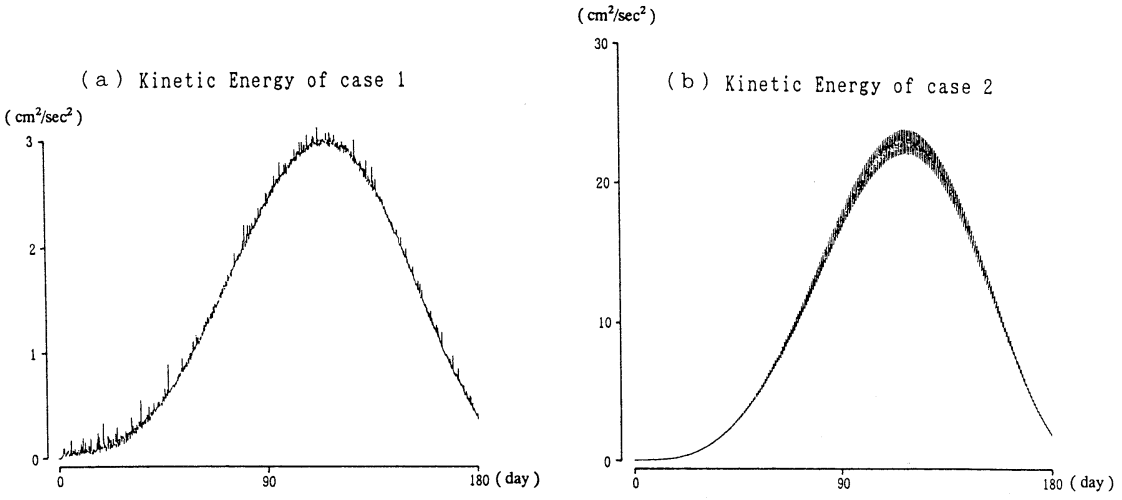

Fig. 3. Time series of the Kinetic energy in Case 1 (a) and Case 2 (b).

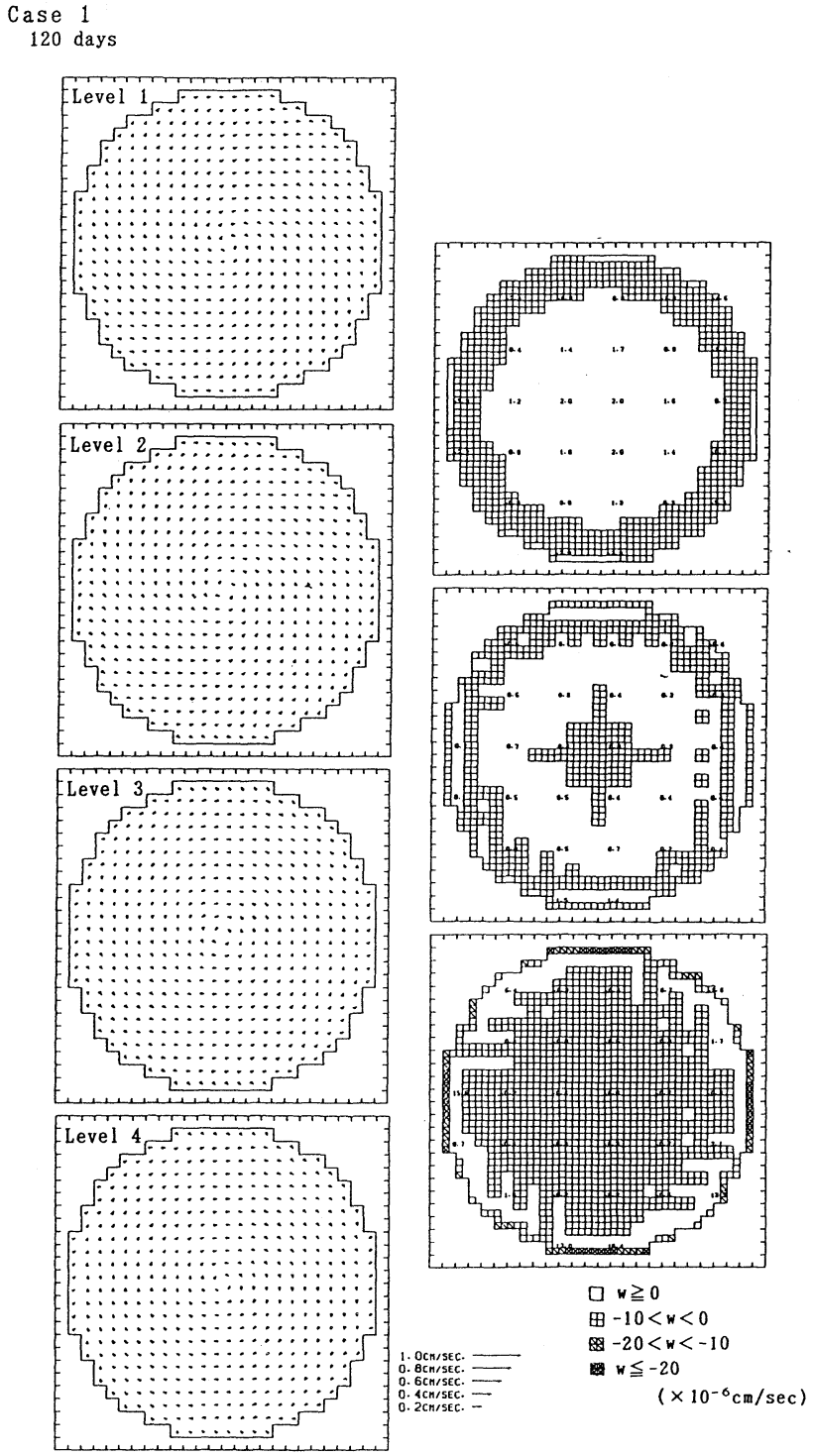

Fig. 4. Horizontal current vectors (left) and vertical current distribution (right) on 120 days of Case 1. Shadow areas show the downwelling.

diffusivity are given as Eq. (14).

2.3. Calculation results

The calculations of all cases are begun from the state of uniform water temperature (5℃), since that is the lowest water temperature in the Yellow Sea in April (TAWARA and YAMAGATA, 1992. see Fig. 1 (c)). Cases of the numerical experiments are shown in Table 2. Figure 3 shows the temporal variations in kinetic energy of Cases 1 and 2 which is defined as

$$KE=\sum_i (u_i^2+v_i^2+w_i^2), \qquad (22)$$

where u_i v_i and w_i are u, v and w at a grid point i, respectively. The kinetic energies of both cases reach to the maximum on about 120 days. So, in this paper, the calculated results on 120 days are shown. Here, the smaller fluctuations of the kinetic energies of both cases have a period of about 20 hours. Since the inertia period is 20.9 hours at 35° N, these flucuations should be accompanied with the inertia motion.

Case 1 is the experiment to investigate the effect of horizontal variation in the vertical mixing due to the tidal current. Figure 4 shows the horizontal (left) and vertical (right) current distributions of Case 1. Clockwise circulations exist in the upper (Level 1) and the loewer layers (Level 4), and an anti-clockwise ones in the middle layers (Levels 2 and 3). Downwelling exists near the lateral wall of the upper layer and at the central part of the lower layer, and upwelling at the central part of the upper layer and near the lateral wall of the lower layer, i.e., the horizontal divergence occurs at the central part of the upper and lower layers and the horizontal convergence at the central part of the middle layer. However, horizontal circulation patterns of Case 1 do not coincide with those of YANAGI and TAKAHASHI (1993). Vertical distribution of water temperature of Case 1 is shown in Fig. 5. This distribution qualitaively reproduce that of Fig. 1 (b), i.e., the highest water temperature exists at the central part of the subsurface and the lowest one at the central part above the sea bottom.

Case 2 is the experiment to investigate the effect of the bottom topography and this experiment is basically the same experiment as OONISHI (1975). Figure 6 shows the horizontal and vertical current distributions of Case 2. An anti-clockwise circulation exists at the upper layers (Levels 1 and 2) and a clokwise one at the lower layers (Lecels 3 and 4). Downwelling exists from the surface to the bottom in the

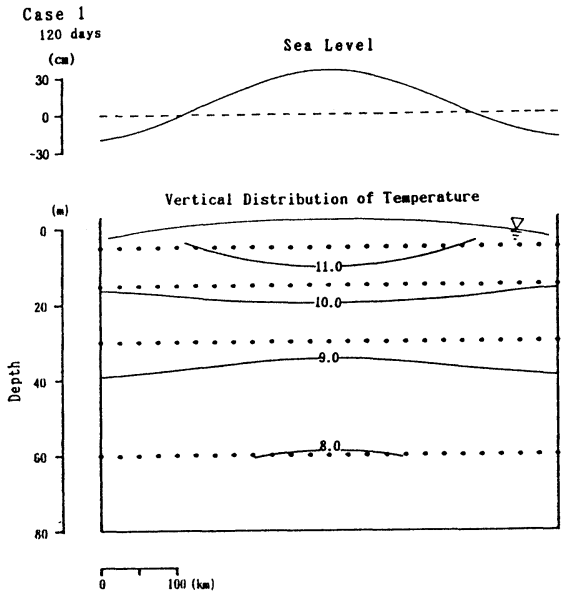

Fig. 5. Vertical distrbution of water temperature on 120 days of Case 1.

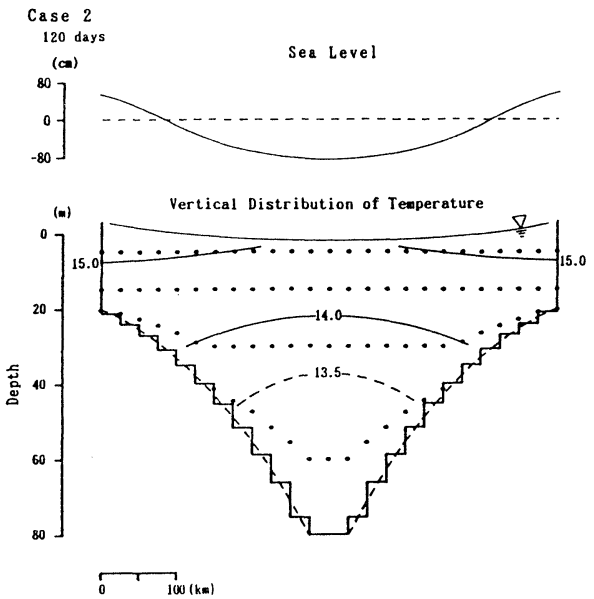

Fig. 7. Vertical distribution of water temperature on 120 days of Case 2.

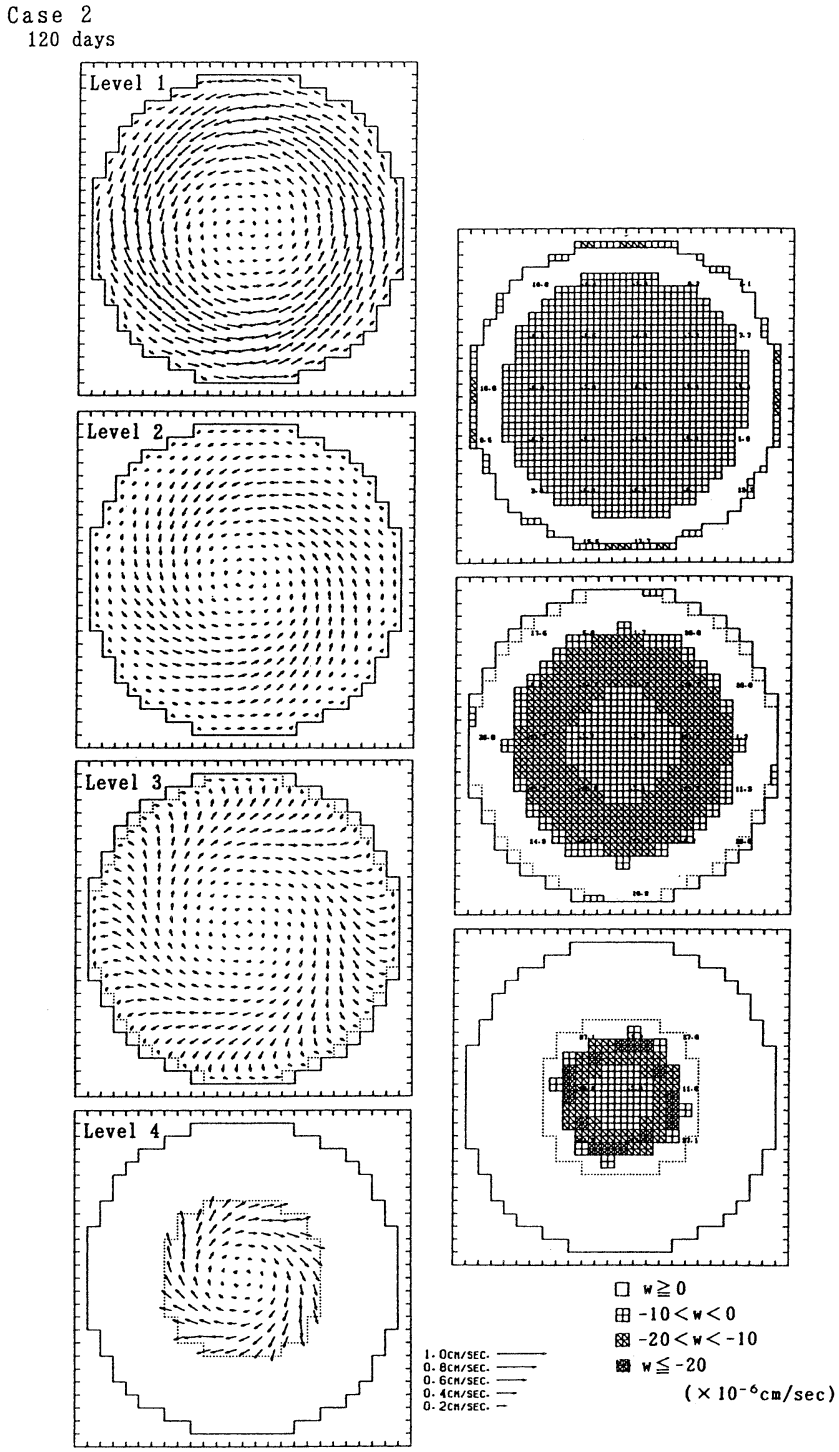

Fig. 6. Horizontal current vectors (left) and vertical current distribution (right) on 120 days of Case 2. Shadow areas show the downwelling.

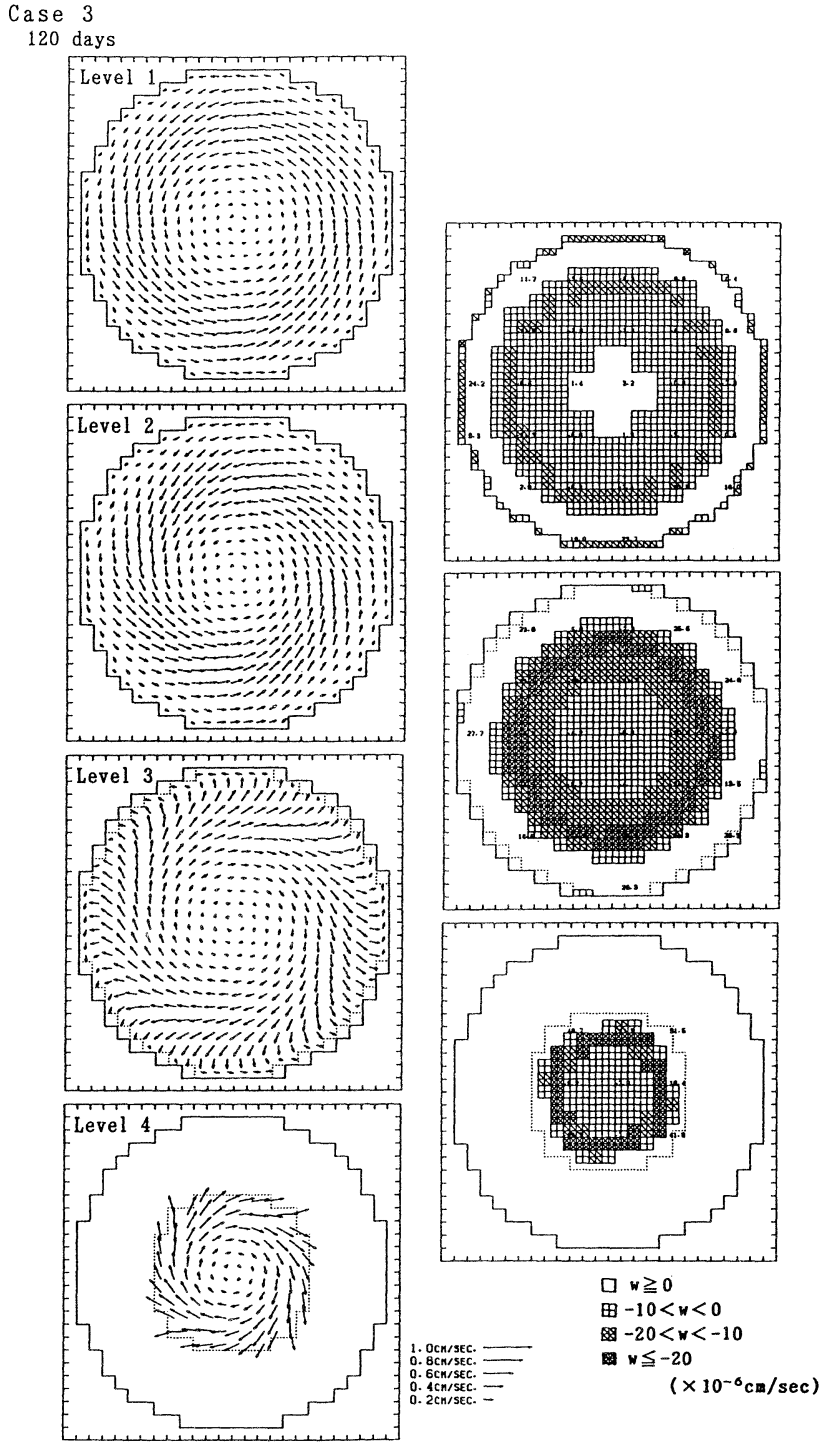

Fig. 8. Horizontal current vectors (left) and vertical current distribution (right) on 120 days of Case 3. Shadow areas show the downwelling.

central part of the basin and upwelling from the surface to the bottom along the lateral wall of the basin, i.e., the horizontal convergence occurs at the central part of the upper layer and the horizontal divergence at the central part of the lower layer. Such horizontal circulation patterns are coincident with those of YANAGI and TAKAHASHI (1993). OONISHI (1975) revealed that such circulations were induced by the topographic heat accumulation effect. Vertical distribution of water temperature of Case 2 is shown in Fig. 7. Water temperature distribution at the upper layer dose not reproduce that of Fig. 1 (b), because the highest water temperature is seen st the sub-surface layer along the side wall. However, the water temperature distribution at the lower layer reproduces that of Fig. 1 (b), because the lowest water temperature exists just above the bottom of the deepest part.

From results of Cases 1 and 2, we can expect that both effects (tidal mixing and bottom topography) contribute to the water temperature distribution and the generation of circulations in the Yellow Sea during summer. Thus, in Case 3, an experiment which takes into account both effects is carried out. Figure 8 shows the horizontal and vertical current distributions of Case 3. Horizontal circulation patterns are coincident with those of Case 2, but the intensity of an anti-cockwise circulation at the upper layer is weaker than that of Case 2. This is resulted from that a weak clockwise circulation at upper layer of Case 1 is superimposed on a strong anti-clockwise one at the upper layer of Case 2. In the upper layer, upwellings exist near the lateral wall and at the central part, and downwelling between upwellings with doughnut-like distribution. In the lower layer, upwelling exists near the lateral wall and downwelling at the central part. This is resulted from that the verical circulations of Case 1 is superimposed on that of Case 2. Figure 9 shows the vertical distribution of water temperature of Case 3. The highest water temperature is seen at the surface layer of the central part and the lowest one just above the bottom of the deepest part. Such distribution pattern reproduces that of Fig. 1 (b), although the developed thermocline is not reproduced. Various kinds of the vertical eddy diffusivities and viscosities which have exponential forms are applied. However, the thermocline is not developed in these experiments.

In Case 4, the vertical eddy viscosity which depends on the Richardson number (Eq. (16))

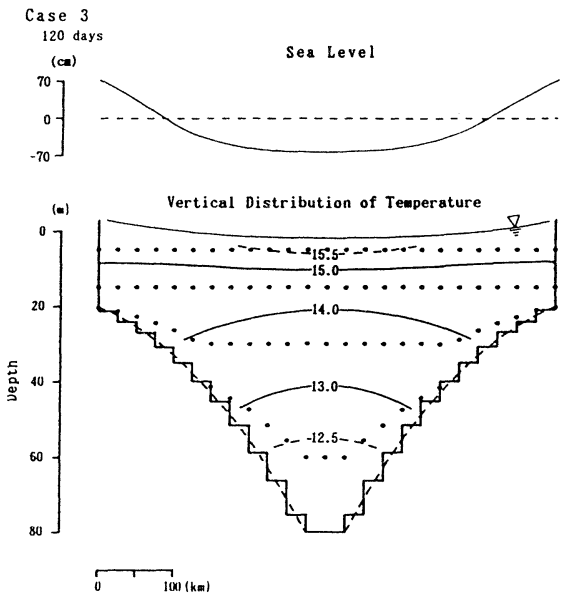

Fig. 9. Vertical distrbution of water temperature on 120 days of Case 3.

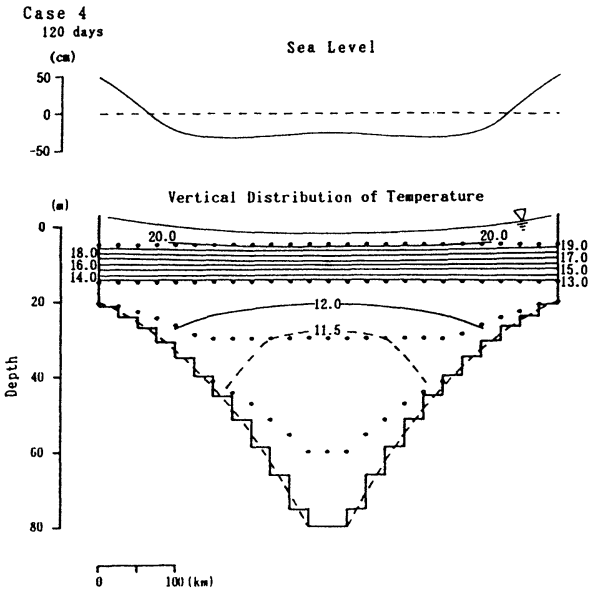

Fig. 10. Vertical distribution of water temperature on 120 days of Case 4.

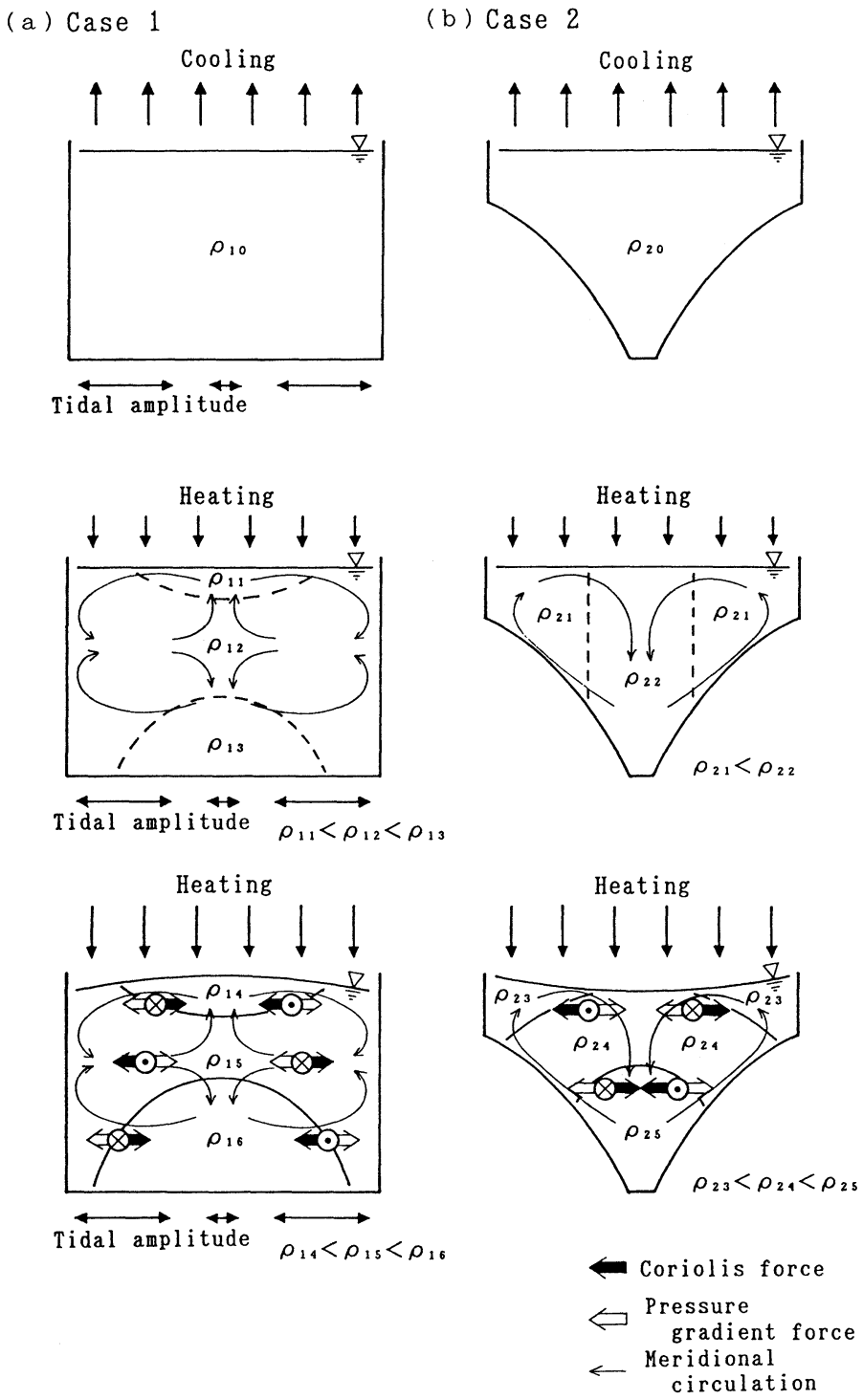

Fig. 11. Schematic figure of the generation mechanisms of the circulations in Case 1 (a) and Case 2 (b).

is applied, i.e., an experiment of Case 4 is carried out in order to reproduce the developed thermocline. Horizontal circulation patterns of Case 4 are coincident wirh those of Case 2, although the intensity of surface anti-clockwise circulation is weak. The vertical water temperature distribution of Case 4 is shown in Fig. 10. The thermocline develops at the sub-surface layer and the low temperature water mass is formed at the bottom of the deepest part of the basin with dome-like shape. Such water temperature distribution well reproduces that of Fig. 1 (b).

3. Discussion and summary

The circulations in the Yellow Sea during summer are mainly induced by the sea surface heating and are affected by the vertical mixing of the tidal current and the bottom topography. The schematic generation mechanisms of the circulations of Cases 1 and 2 are shown in Fig. 11. In Case 1, the homogeneous water which is formed by the sea surface cooling in winter begins to stratify due to the sea surface heating in spring. However, due to the horizontal difference of the tidal vertical mixing effect, the intensity of the stratification in the central part of the basin becomes stronger than that of surrounding part. Thus, the lightest (highest temperature) and the heaviest (lowest temperature) waters are formed at the upper and lower layers in the central part of the basin. such density distrbution drives the horizontal divergences at the upper and lower layers and the horizontal convergence at the middle layer. Accompanied by such horizontal divergences and convergence, the water column in the central part is shrunk at the upper and lower layers and is stretched at the middle layer, i.e., in the central part of the basin, the water column at the upper and lower layers obtain the negative relative vorticity and that at the middle layer obtain the positive relative vorticity due to the conservation law of potential vorticity in the rotational fiuid. Consequently, the clockwise circulations are developed at the upper and lower layers and an anti-clockwise one at the middle layer. Here, the largest vertical velocity of the Case 1 has an the order of 10^{-5} c m/sec. So, the vertical maximum movement of the water particles are only several meters per 180 days, i.e., the water particles obtain the positive (negative) relative vorticity at eyery time during heating season. Hence, the horizontal circulations of Case 1 are maintained during heating season with the structure of the quasi geostrophic current and the sea level of the central region rises due to the geostrophic adjustment.

In Case 2, the initial condition is the same as that of Case 1. At the beginning of the surface heating, the lighter (higher temperature) water is distributed on the shallow area and the heavier (lower temperature) water in the central deeper part due to the topographic heat accumulation effect. Such density distribution drives the horizontal convergence in the upper layer and the horizontal divergence in the lower layer. Accompanied by such horizonatal convergence and divergence, the water colnmn in the central part is stretched in the upper layer and is shrunk in the lower layer, i.e., in the central part of the basin, the water column at the upper layer obtains the positive relative vorticity and that at the lower layer obtains the negative relative vorticity. Consequently, an anti-clckwise circalation is developed at the upper layer and a clockwise one at the lower layer. Here, the largest vertical velocity of the Case 2 has an order of 10^{-5} cm/sec. So, the vertical maximum movement of the water particles are only several meters per 180 days, i.e., the water particles obtain the positive (negative) relative vorticity at every time during heating season. Hence, the horizontal circulations of Case 2 are maintained during heating season with the structure of the quasi geostrophic currrent and the sea level of the central region falls due to the geostrophic adjustment.

From the water temperature distribution in Fig. 1 (b) and the summer circulations pattern of YANAGI and TAKAHASHI (1993), it is concluded that the generation mechanisms of the circulation in the Yellow Sea during summer correspond to those of both Cases 1 and 2 (i.e. Case 3), although the mechanism of Case 1 weaken the intensity of an anti-clckwise circulation at the upper layer. Furthermore, the thermocline which is not reproduced in the experiment of Case 3 is well reproduced in the

experiment of Case 4 using the vertical eddy diffusivity which depends on the Richardson number, i.e., it is revealed that not only the horizontal distribution of the vertical eddy diffusivity but also the verical one plays an important role in the formation of the water temperature distribution in the Yellow Sea during summer.

The generation mechanisms of the circulations in the Yellow Sea during summer is revealed using a numerical model with simplified model basin. In this study, the horizontal heat flux between the Yellow Sea snd the East China Sea is ignored. However, TAKEOKA *et al.* (1991) revealed the importance of the horizontal heat process in the fomation of the density stratification in Hiuchi-Nada of the Seto Inlando Sea, Japan. So, we have consider the horizontal heat flux effect to the formation of the density stratification and the circulations of the Yellow Sea during summer in future.

Acknowledgements

The authors wish to express their sincere thanks to Dr. H. TAKEOKA and Mr. H. AKIYAMA of Ehime University and Dr. Y. ISODA of Hokkaido University for their helpful discussions. The numerical experiments were carried out on a FACOM M-770 of the Computer Center of Ehime University.

References

CHOI, B. H. (1984): A three-dimensional model of the East China Sea. p. 209-224.: *In* Ocean Hydrodynamics of Japan and East Cina Seas, T. ICHIYE (ed.) Elsevier, Amsterdam.

CHOI, B. H. and H. J. LIE (1992): Physical oceanography program of the East China Sea and the East Sea (Japan Sea) dynamics in Korea. Proceeding of PORSEC-92, 1-28.

FUKASE, S. (1975): Bottom water on the continental shelf in the East China Sea. Umi to Sora (Sea and Sky), **51**, 13-15. (in Japanese)

ISHII, T. and J. KONDO (1987): Seasonal variation of the heat balance of the East China Sea. Tenki (Weather), **34** (8), 517-526. (in Japanese)

ISHII, T. and J. KONDO (1993): Seasonal variation of the heat balance of the East China Sea and its vicinity — Ocean heat transport and Ocean storage of heat —. Tenki (Weather), **40** (5), 309-324. (in Japanese)

JAMES, I. D. (1977): A model of the annual cycle temperature in the frontal regin of the Celtic Sea. Estuarine, Coastal Marine Sci., **5**, 339-353.

OONISHI, Y. (1975): Development of the current induced by the topographic heat accumulation (1) — The case of the axisymmetric basin —. J. Oceanogr. Soc. Japan, **31**, 243-254.

SU, Y. S. and X. C. WENG (1994): Water masses in China Seas. p. 3-16. *In*: Oceanography of China Seas. 1, ZHOU, D. *et al.*, (eds,), Netherlands.

TAKEOKA, T., Y. OHNO and N. INAHATA (1991): Roles of horizontal processes in the formation of density straification in Hiuchi-Nada. J. Oceanogr. Soc. Japan, **47**, 33-44.

TAWARA, S. and T. YAMAGATA (1991): Seasonal formation of bottom water in the Yellow Sea and its interannual variability. Umi to Sora (Sea and Sky), **66**, 273-282. (in Japanese)

WADACHI, K. (ed.) (1987): Encyclopedia of Oceanography. Tokyodo-Press, Tokyo, 589 pp.

YANAGI, T and S. TAKAHASHI (1993): Seasonal variation of circulations in the East China Sea and the Yellow Sea. J. Oceanogr., **49**, 491-501.

夏季の黄海の循環流の生成機構に関する数値研究

高橋　暁 • 柳　哲雄

要旨：柳，高橋（1993）は夏季黄海では表層で反時計回り，底層で時計回りの循環流が発生することを明らかにした。この循環流の生成機構を明らかにするために単純な地形の数値実験を行った。その結果，この循環流は主に地形性貯熱効果により生成すること，水温鉛直分布には潮流による鉛直拡散の水平的違いが影響していることがわかった。